

**DIBLOCK COPOLYMER LAMELLAE EMERGING PATTERNS WITH
CELL DYNAMIC SIMULATIONS USING DIAGONAL
DISCRETIZATION METHOD OF LAPLACIAN WITH 9-POINT STENCIL
IN POLAR MESH SYSTEM**

Muhammad Javed Iqbal^{1*}	mjaved.iqbal@salu.edu.pk	https://orcid.org/0009-0000-1737-1826
Inayatullah Soomro¹	inayat.soomro@salu.edu.pk	https://orcid.org/0000-0001-6423-1009
Usama Gulzar¹	usama.gulzar@salu.edu.pk	https://orcid.org/0009-0007-1353-1272
Muhammad Salman Javed¹	salman.javed@salu.edu.pk	https://orcid.org/0009-0003-9207-951X

¹Department of Mathematics, Shah Abdul Latif University Khairpur, Sindh, Pakistan.

^{1*}Corresponding Author

ABSTRACT

The use of soft materials in nanotechnology is revolutionizing the industry. Given their special importance in soft and advanced functional materials, theoretical researchers are presenting their studies in search of new equilibrium configuration phases in diblock copolymer systems. In this regard, prospective research has predicted lamella morphologies in new nanostructures through mathematical modelling and simulations. Confinement has also been applied to enable new emerging nanostructure patterns by establishing a surface field. The choice of a fast and efficient cell dynamic simulation model to observe the role of order parameters between two incompatible blocks of a diblock copolymer system distinguishes it from other prevailing models. In this study, we present a new diagonal approximation method to discretize the macromolecule of the diblock copolymer system in polar geometries. A new diagonally discretized 9-point stencil has been numerically formulated for simulation in the CDS model after developing a FORTRAN code for a set of PDEs involved in the CDS model. The new confined nano-particle patterns are presented by visualizing numerical data using OPENDX. Comparison of the proposed study with existing studies validates and distinguishes the research from the proposed studies.

1. Introduction

Nanotechnology involves designing new materials by engineering and manipulating soft materials at the nanoscale [1-4]. Soft materials, including polymers, colloids, surfactants, and liquid crystals, can be easily deformed due to their self-assembly properties [5-6]. The combination of soft

materials and nanotechnology has enabled access to new biomaterials, miniature robots, multi-sensor devices, and high-density storage media [7-9]. Diblock copolymers are among the most interesting advanced functional materials recognized as having an important role in altering and advancing the industry with nanotechnology [10-12]. These materials are formed by the covalent bonding of two thermodynamically different polymer chains, as shown in Figure 1. In diblock polymer systems, polymers formed from one type of monomeric chain are shown in red, and polymers formed from the other monomeric chain are shown in blue [13-14].

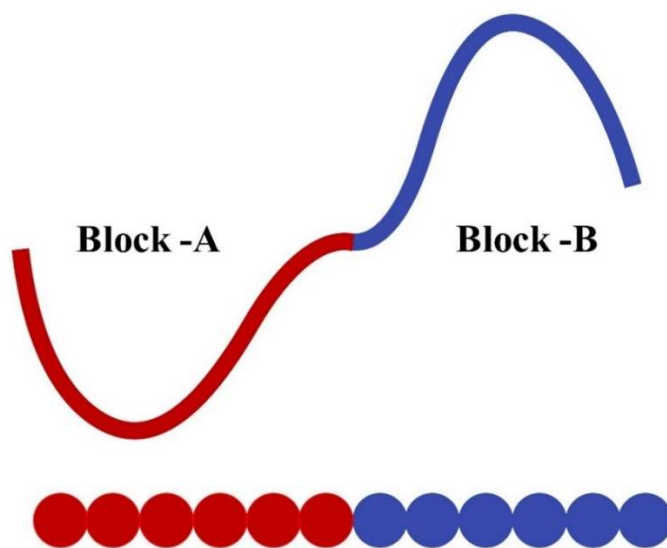


Figure 1: Diblock copolymers

Self-assembly and phase separation from spontaneous joining led to its various morphologies, with lamellar morphology arising from the tendency of each polymer block to separate into distinct regions due to the incompressible behaviour of each polymer block [15-18]. Lamellar morphologies have promising applications in nanotechnology due to their defined patterns and tunable properties. These applications include nanolithography, directed self-assembly, media of energy storage, selective permeability of membranes and drug delivery [19-21]. Achieving precise control over the orientation, periodicity and defect density of the lamellar morphology of diblock polymer systems in polar geometries, the mass production of defined lamellar structures for physical applications and mathematical modelling of lamella patterns to integrate them with other inorganic nanoparticles and electronic components to fabricate multifunctional devices are challenging [22]. Diblock copolymer systems consist of two inherently incompatible blocks of

polymers that spontaneously form self-organized periodic nanostructures in bulk due to a balance between chain stretching energy and interfacial energy. The structures include alternating lamellae, complex bicontinuous gyroid, hexagonally packed cylinders, and cubic arrays of spheres, shown in Figure 2. These morphologies are tuned by the architecture, composition, volume fraction, interaction between the segments of the constituent block in the system, and surface properties applied to the system.

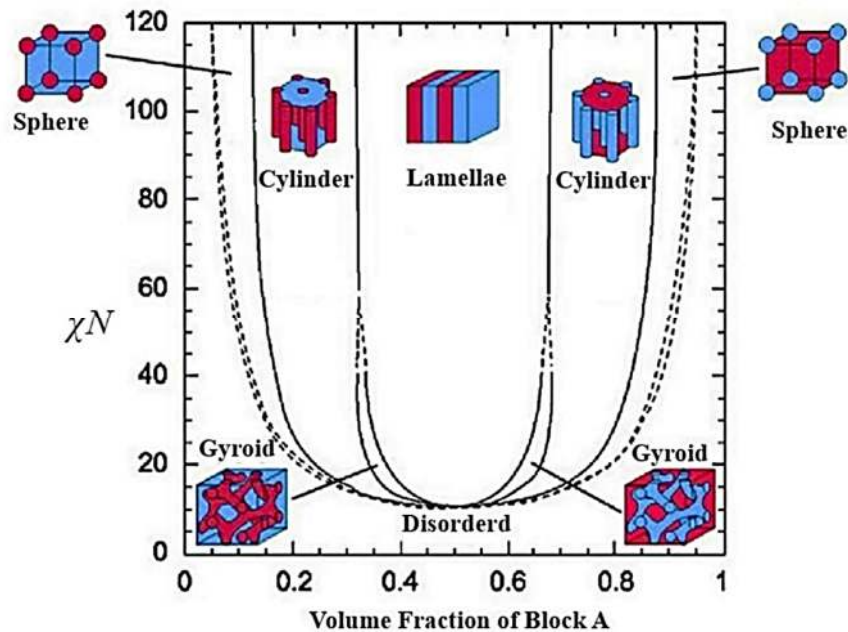


Figure 2: equilibrium phases of Diblock copolymers

The bulk phase diagram in the figure shows the degree of segregation as a function of volume fraction in a diblock copolymer system, showing ordered phases with different equilibria. N refers to the degree of polymerization, which determines the size of the polymer segment and χ refers to the interaction between the two blocks. The product of χ and N is called the degree of segregation χN , inversely proportional to the temporal parameter τ . Keeping the value of the volume fraction of each block at 0.5 and the value of χN at 10.2 gives us the lamella formulation. [23-25]. Soft materials require uniform alignment with long ranges for many applications that require manipulation of self-assembly. Various approaches are used for this, including shearing [26], phase separation under confinement [27], directing the assembly of the electric field [28-29], magnetic field [30], and controlling the dynamics by exploiting temperature gradients [31]. Bulk

equilibrium can be broken by introducing external forces. Among these external constraints, geometrical confinement has its distinctive place. Geometric confinement reorients the compatibility between the confinement surface and the bulk polymer period, making new morphologies inaccessible in the bulk phase. Confinement involves bringing a block to the surface under preferential attraction by the surface field, bringing parallelism to the interface and equal spacing of the microdomains. The geometry of confinement influences nanoscale geometrical templates of Lamellae morphology. This geometrical constraint introduces topological constraints that tend to frustrate preferred structures. These geometrical constraints dictate the reorganization of the nanostructure template by minimizing the interfacial energy and conforming the lattice to the geometry [32]. Aggregating diblock copolymer systems in polar confinement introduce asymmetric topological constraints that cannot be observed in the bulk. Confinement in this geometry examines the disruption of the lamellae under the influence of angular and radial gradients. Confining the diblock copolymer system to a polar geometry forces the microdomains to be closely packed and aligned at low-thickness sites to reduce the interfacial area due to the geometry. The simulations allow the generation of morphologies that can produce perturbation effects in the polarized architecture of radially coherent layers. Confinement relaxation leads to interlayer gaps and their orientational symmetry due to increased thickness around the wedge. Confinement in polar geometry induces strong enough frustration to induce self-assembly of the system into incoherent structures and to break structural symmetries. Diblock polymer systems undergo self-assembly during confinement in a circular annular pore, breaking the symmetry and causing frustration due to the geometrical topology. Confinement is stronger at the center of the disc, at which point the microphase-separated morphology is brought to minimum energy, and the lamellar arrangement and layers are combined [33]. Cell dynamic simulation is advantageous over other methods because it works efficiently on long-range orders. It is used for better results with little compromise on its computational cost [34]. Given the importance of the Laplacian in the CDS model, macromolecules are discretized by transforming them into discrete set-of points. Lamellae morphology was investigated by Iqbal et al. (2024) by using isotropic discretization of Laplacian in the polar mesh with cell dynamic simulations [35]. The effect of confinement on diblock copolymer melts was investigated by Iqbal et al. (2024) in spherical order structures [36] and investigated the impact of one-dimensional confinement in cylindrical geometries [37]. Lamella morphologies in diblock polymer systems have not been studied much in computational modeling

in polar geometry. In previous studies, a thorough investigation of the results in the presence of error and anisotropy was lacking. Previous studies have not fully identified lamella alignment and structure defects in irregular boundaries. It is also important to validate the asymmetric lamella study with experimentally prepared lamellas included in this study. More significant lamella patterns are made possible by using a numerical scheme based on diagonal discretization in polar geometry in simulations to reduce error and improve the confinement and curvature effects. Confinement-induced lamella structures are of utmost importance in nanotechnology due to their importance in polymer science [38-40]. Cohesion of lamellae in the melt imposes a strong preferential surface to form a concentric lamella (CL) forming system. Various simulation systems have been used in the mathematical modeling of diblock copolymer systems to investigate concentric lamella (CL) forming systems, including MCS [41], DDFTS [42], DPD [43], TEM [44], SST [45] and SCFT [46-48].

From this literature survey, it has been revealed that a combination of discrete simulation methods and mathematical models has predicted concentric circular lamella patterns. Still, circular lamella patterns of asymmetric diblock copolymer systems have not been predicted using cell dynamic simulation models and diagonal discretization of the Laplacian. Realizing this research gap, the present investigation has been conducted to understand better concentric lamellae formed by curvature, geometry, change in thickness, and confinement effects in the diblock copolymer system on large-scale simulation. In this study, we aim to identify novel structures of concentric lamellas by examining weak and strong segregation at different pore diameters. The first part of the present research study presents the applicability, need, and understanding of diblock copolymer systems in nanotechnology in light of previous investigations. The next section describes an overview of the cell dynamic simulation model and procedure, including the steps to discretize the Laplacian diagonally. Concentric lamella formations with and without confinement are discussed in the third section. In the last stage, a comparison and contrast of this research and different researchers have been presented.

2. Materials and Methods

2.1 Diagonal discretization of AB-diblock copolymer macromolecule

Diblock is presented to approximate an isotropic Laplacian by converting the continuous domain of the polymer system into a discrete set of coordinates in a polar grid system by finite difference

method, and an isotropic Laplacian approximation is presented for a 9-point stencil. A numerical scheme is developed, as shown in Figure 3. The periodic boundary conditions are in the radian angular domain $0 < \theta < 2\pi$ and the reflective boundary conditions are analogous to the radial domain. The discrete domains along the radial axis are spaced as Δr and the radian axis as $\Delta\theta$. The annular polar grid is implemented to avoid singularity problems under a circular annular pore system. A polar pore system consists of a fixed inner radius r_a and a variable outer radius r_b . The equation involving pore is are given as

$$d = r_b - r_a \tag{1}$$

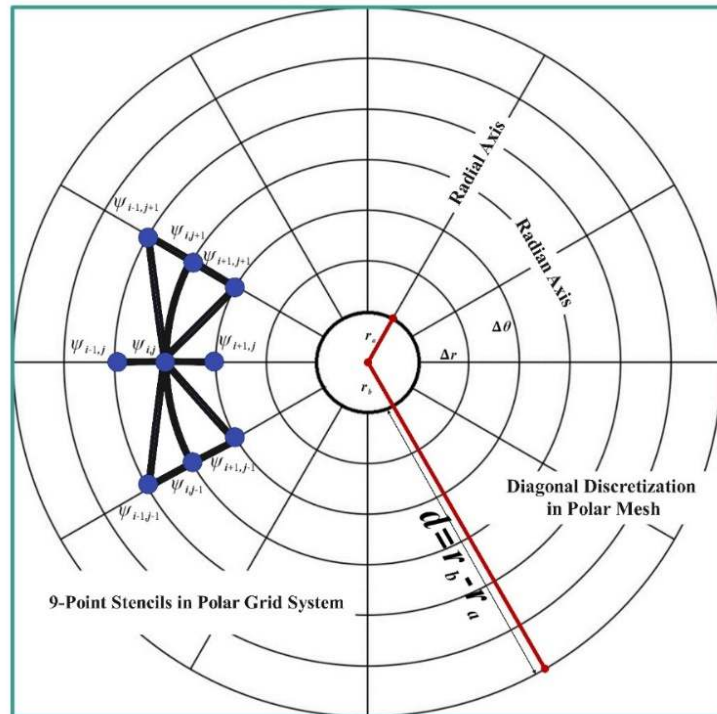


Figure 3: Diagonal Discretization in polar mesh

This paper presents a diagonal discretization method instead of normal discretization to reduce errors and increase the simulation capability. In Figure 3, a 9-point diagonally discretized stencil is presented with an average point $\psi_{i,j}$ of four neighbouring points $\psi_{i-1,j}$, $\psi_{i+1,j}$, $\psi_{i,j-1}$ and $\psi_{i,j+1}$ and four nearest neighbouring points $\psi_{i+1,j+1}$, $\psi_{i-1,j-1}$, $\psi_{i+1,j-1}$ and $\psi_{i-1,j+1}$. These mixed nearest neighboring points are diagonally connected to the averaging point. This reduces error and consequently improves the approximation of the polar geometry.

The Laplacian involved in the CDS model is defined as:

$$\nabla^2 = S + O_1(h_1^n) + O_2(h_2^n) \quad (2)$$

In this Laplacian, S is stencil and $O_1(h_1^n), O_2(h_2^n)$ are truncation errors with mesh sizes h_1 and h_2 respectively. The proposed stencil satisfies the conditions:

$$\sum_{r=1}^3 \sum_{\theta=1}^3 S_{r,\theta} = 0 \quad (3)$$

The discrete i^{th} radial space r_i is defined as

$$r_i = r_a + i\Delta r \quad \text{for} \quad i = 1, 2, 3, \dots, N_r \quad (4)$$

The discrete j^{th} radian space θ_j is defined as

$$\theta_j = j\Delta\theta \quad \text{for} \quad j = 1, 2, 3, \dots, N_j \quad (5)$$

2.2 The Simulation Model (CDS)

A cell dynamic simulation model is applied to a diblock polymer system to examine cell interactions under a domain-distributed grid and the concentration in the cell space, shown in . The model predicts the lamella patterns in principle by minimizing the free energy. A macromolecule of diblock copolymer melt FORTRAN codes computes the partial differential equations involved in the CDS model. A 9-point diagonal discretized stencil has been fine-tuned to obtain better simulations with the help of the CDS model. The investigated patterns are validated by predicting lamella morphology. These predicted patterns, with or without confinement, are compared with existing computationally and experimentally lamella patterns.

A diblock copolymer system consists of two blocks A and B with a macromolecule consisting of N polymer chains. The length of each block is represented by N_α ($\alpha = A$ or $\alpha = B$) containing f_α monomers, α is species of monomers in the form of $f_\alpha Z$ statistical segments with $l n^{\frac{1}{2}}$ scale length (l is Kuhn length).

In diblock copolymer system, the local volume fraction ϕ_α refers to the concentration of a block in a specific area of the material relative to the total volume. This parameter specifies how much of the block is in a specific region or material phase during simulation.

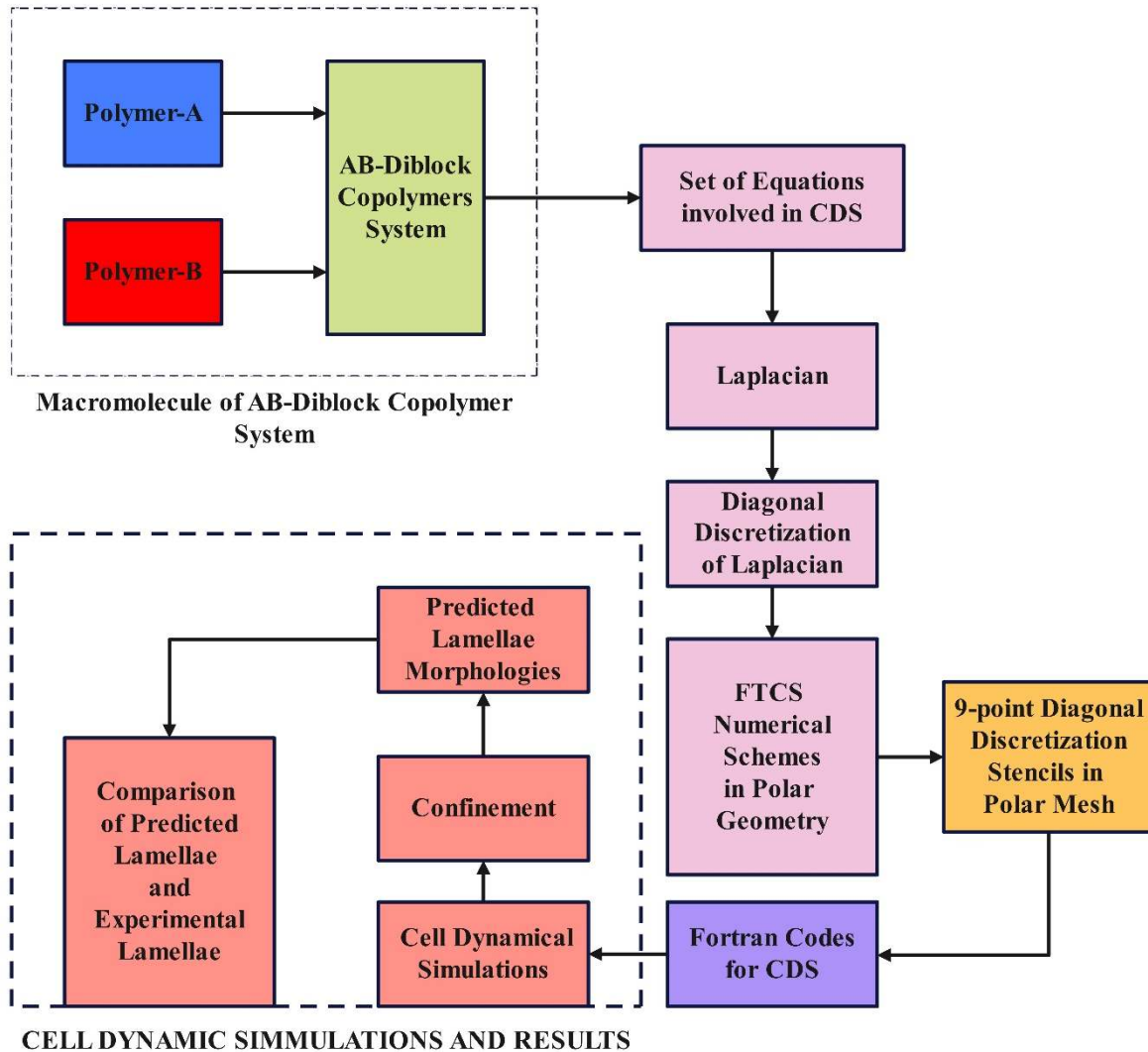


Figure 4: Diagonal Discretization in polar mesh

In the process of microphase separation, these two blocks are from distinct domains, and the spatial volume fraction helps to characterize these domains' size, shape, and distribution. Theoretical models and simulations of diblock copolymers make it possible to account for local variations by local volume fraction in predicting the material's morphology, mechanics, and self-assembly behaviors. The global volume fraction is the total volume of the simulation box. It is defined in the initial setup of the simulation. It represents the overall size of the system and quantifies the overall properties of the system.

The local volume fraction of each block in the system is given as

$$\varphi_A = \frac{1}{\rho_0} \sum_{i=1}^N \int_0^{f_A} d\zeta \delta\{r - r_i^A(\zeta)\} \quad (6)$$

$$\varphi_B = \frac{1}{\rho_0} \sum_{i=1}^N \int_0^{f_B} d\zeta \delta\{r - r_i^B(\zeta)\}. \quad (7)$$

ρ_0 is the density of melt connectivity, ζ is the temporal parameter, $0 < \zeta < N$ and δ is an incompressibility constraint. Cell dynamic simulation techniques use order parameters $\psi(i, t)$ for each i cell and t time to represent the properties of each computational cell involved in the microstructure [49-50]. The order ψ is computed for the AB diblock copolymer using the difference between the local and global volume fractions:

$$\psi = \phi_A - \phi_B + (1 - 2f). \quad (8)$$

ϕ_A and ϕ_B are local volume fractions of A and B monomers, respectively. The global volume fraction is defined as:

$$f = \frac{N_A}{N_A + N_B}. \quad (9)$$

Considering the difference between local and global volume fractions allows us to explore the spatial distribution of polymer chains, capture the effects of chain packing and interactions, and gain insights into the phase behaviour and self-assembly of diblock copolymer systems.

Any change in the order parameter over time must meet the requirements of the following equation to provide continuity:

$$\frac{\partial \psi(r, t)}{\partial t} = -\nabla \cdot j(r, t) \quad (10)$$

This equation assumes that $j(r, t)$ is a flux that is linearly connected to the local chemical potential:

$$j(r, t) = -M\nabla\mu(r, t) \quad (11)$$

The functional derivative of the free energy in the following way gives the chemical potential:

$$\mu(r, t) = \frac{\delta F[\psi]}{\delta \psi} \quad (12)$$

The Cahn-Hilliard-Cook (CHC) equation describes the order parameter's time evolution:

$$\frac{\partial \psi}{\partial t} = M\nabla^2 \left(\frac{\delta F[\psi]}{\delta \psi} \right) + \eta \xi(r, t) \quad (13)$$

In this equation (5), $M = 1$ represents the mobility coefficient, η is the noise amplitude and $\xi(r, t)$ is a Gaussian white noise with zero mean and unit variance. In this investigation, it is observed that $\eta \xi(r, t)$ does not significantly impact the simulation results, so the noise term is not programmed in the simulations.

In the derivation of the free energy, all the terms have a physical meaning. Even though the free energy is, of course, mesoscopic and coarse-grained and thus it is only an approximation [51].

The free energy functional $F[\psi(r)] \div kT$ is represented by the equation:

$$F[\psi(r)] = \int dr \left[H(\psi) + \frac{D}{2} |\nabla\psi|^2 \right] + \left(\frac{B}{2} \right) \int dr \int dr' G(r - r') \psi(r) \psi(r') \quad (14)$$

$F[\psi(r)]$ has two terms. The first part $\int dr \left[H(\psi) + \frac{D}{2} |\nabla\psi|^2 \right]$ of $F[\psi(r)]$ is identical to the Ginzburg–Landau free energy used to describe phase separation in a binary mixture. The second part $F[\psi(r)]$ of $F[\psi(r)]$ represents the long-range interactions arising from the connectivity of different blocks in a copolymer [47]. D is a positive constant for the diffusion coefficient. $G(r - r')$ is a green function for Laplacian, satisfies $\nabla^2 G(r - r') = -\delta(r - r')$ [52].

The parameter B introduces a chain-length dependence to the free energy $H(\psi)$ [53], given as

$$H(\psi) = \left[\left(-\frac{\tau}{2} \right) + \left(\frac{A}{2} \right) (1 - 2f)^2 \right] \psi^2 + v(1 - 2f) \psi^3 + \left(\frac{u}{4} \right) \psi^4 \quad (15)$$

The temperature parameter is represented by τ , while A , v , and u are phenomenological constants. $\tau' = -\tau + A(1 - 2f)^2$, D , and B can be expressed in terms of the degree of polymerization N , the segment length b , and the Flory-Huggins parameter χ , which is inversely proportional to temperature. The χ -parameter is used to measure the relative strength of the repulsion ($\chi > 0$) and attraction ($\chi < 0$) between the same types of segments. The expressions for τ' , D , and B are given by:

$$\tau' = \left(-\frac{1}{2N} \right) \left(N\chi - \frac{s(f)}{4f^2(1-f)^2} \right) \quad (16)$$

$$D = \frac{b^2}{48f(1-f)} \quad (17)$$

$$B = \frac{9}{4N^2 b^2 f^2 (1-f)^2} \quad (18)$$

The numerical evolution of CDS equation (2) by finite difference scheme for order parameter is:

$$\psi(\mathbf{n}, t + 1) = \psi(\mathbf{n}, t) - \{ \langle \langle \Gamma(\mathbf{n}, t) \rangle \rangle - \Gamma(\mathbf{n}, t) \} + B\psi(\mathbf{n}, t) - \eta\xi(\mathbf{n}, t). \quad (19)$$

Where $\Gamma(\mathbf{n}, t) = g(\psi(\mathbf{n}, t)) - \psi(\mathbf{n}, t) + D[\langle \langle \psi(\mathbf{n}, t) \rangle \rangle - \psi(\mathbf{n}, t)]$. (20)

$\{ \langle \langle \Gamma(\mathbf{n}, t) \rangle \rangle \} - \Gamma(\mathbf{n}, t)$ is isotropized discrete Laplacian [48] in polar and $i = (i_r, i_\theta)$ are polar coordinates with Δt time steps for order parameters.

In case of confinement

$$\Gamma(\mathbf{n}, t) = g(\psi(\mathbf{n}, t)) - \psi(\mathbf{n}, t) + D[\langle \langle \psi(\mathbf{n}, t) \rangle \rangle - \psi(\mathbf{n}, t)] - s_i(r). \quad (21)$$

Here $s_i(r) = h_i \times \phi_i \times \delta_{n_r=1 \text{ or } n_r=N_r}$.

The strength of the mutual interaction of walls and blocks is h_i . The Kronecker delta, represented by $\delta_{n_r=1 \text{ or } n_r=N_r}$. This equation is the product of the total segments h_i , the local volume fraction ϕ_i , and the Kronecker delta function $\delta_{n_r=1 \text{ or } n_r=N_r}$. This equation is used to calculate the local segment density at the r position of the specified i block. The Kronecker delta function ensures that the fractional density contribution comes only from cells at the boundaries of the system ($n_r = 1$ or $n_r = N_r$), so that these cells are more likely to be interfaces or boundaries between different blocks.

The discretization of the free energy function $g(\psi)$ is given by:

$$g(\psi) = [1 + \tau - A(1 - 2f)^2]\psi - v(1 - 2f)\psi^2 - u\psi^3. \quad (22)$$

We know the Laplacian in polar form

$$u_{rr} + \frac{1}{r}u_r + \frac{1}{r^2}u_{\theta\theta} = \nabla^2 \quad (23)$$

Here we take $0 \leq \theta \leq 2\pi$ with $\theta_j = j\Delta\theta$ for $i = 1, 2, 3, \dots, n_r$ and $r_a \leq r \leq r_b$ with $r_i = r_a + i\Delta r$ for $j = 1, 2, 3, \dots, n_\theta$. The discretization of a continuum molecule of the diblock copolymer system into discrete set-off points is accomplished by the finite difference approach for the Laplacian used in the CDS model in the polar mesh. The following are the discrete 9-point isotropic stencils for the Laplacian in the polar grid:

The macromolecule of the diblock copolymer system discretized diagonally in the polar mesh system is given in Figure 5.

The first-order approximation for the points $\psi_{i-1,j}$, $\psi_{i,j}$ and $\psi_{i+1,j}$ with respect to the radial axis is:

$$\psi_r = \frac{1}{2(\Delta r)}\{\psi_{i+1,j} - \psi_{i-1,j}\}. \quad (24)$$

The first-order approximation for the points $\psi_{i+1,j+1}$, $\psi_{i,j}$ and $\psi_{i-1,j-1}$ for the radial axis is:

$$\psi_r = \frac{1}{2\sqrt{(\Delta r)^2 + (\Delta\theta)^2}}\{\psi_{i+1,j+1} - \psi_{i-1,j-1}\}. \quad (25)$$

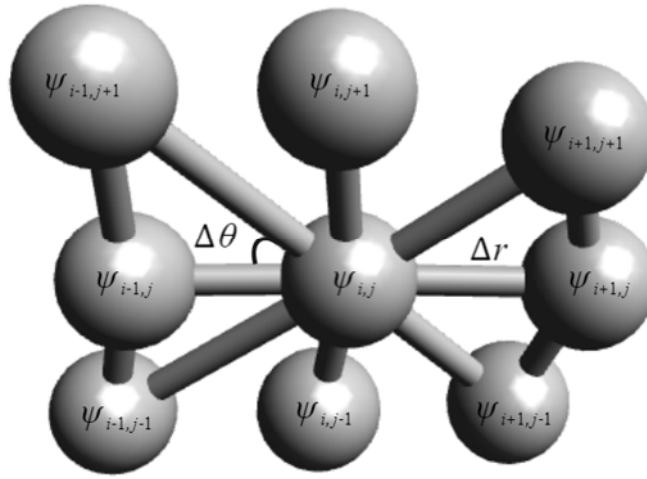


Figure 5: A 9-point discrete macromolecule of diblock copolymer system.

The first-order approximation for the points $\psi_{i-1,j+1}$, $\psi_{i,j}$ and $\psi_{i+1,j-1}$ for the radial axis is:

$$\psi_r = \frac{1}{2\sqrt{(\Delta r)^2 + (\Delta \theta)^2}} \{\psi_{i-1,j+1} - \psi_{i+1,j-1}\}. \quad (26)$$

By adding (24), (25) and (26), we have the first-order approximation of diagonal discretized 9-point stencils concerning the radial axis:

$$\psi_r = \frac{1}{6(\Delta r)} \{\psi_{i+1,j} - \psi_{i-1,j}\} + \frac{1}{6\sqrt{(\Delta r)^2 + (\Delta \theta)^2}} \{\psi_{i+1,j+1} - \psi_{i-1,j-1} + \psi_{i-1,j+1} - \psi_{i+1,j-1}\}. \quad (27)$$

The second-order approximation for the points $\psi_{i-1,j}$, $\psi_{i,j}$ and $\psi_{i+1,j}$ for the radial axis is:

$$\psi_{rr} = \frac{1}{(\Delta r)^2} \{\psi_{i+1,j} - 2\psi_{i,j} + \psi_{i-1,j}\}. \quad (28)$$

The second-order approximation for the points $\psi_{i+1,j+1}$, $\psi_{i,j}$ and $\psi_{i-1,j-1}$ for the radial axis is:

$$\psi_{rr} = \frac{1}{\{(\Delta r)^2 + (\Delta \theta)^2\}} \{\psi_{i+1,j+1} - 2\psi_{i,j} + \psi_{i-1,j-1}\}. \quad (29)$$

The second-order approximation for the points $\psi_{i-1,j+1}$, $\psi_{i,j}$ and $\psi_{i+1,j-1}$ for the radial axis is:

$$\psi_{rr} = \frac{1}{\{(\Delta r)^2 + (\Delta \theta)^2\}} \{\psi_{i-1,j+1} - 2\psi_{i,j} + \psi_{i+1,j-1}\}. \quad (30)$$

By adding (28), (29) and (30), we have the second-order approximation of diagonal discretized 9-point stencils concerning the radial axis:

$$\psi_{rr} = \frac{1}{3(\Delta r)^2} \{\psi_{i+1,j} - 2\psi_{i,j} + \psi_{i-1,j}\} + \frac{1}{3\{(\Delta r)^2 + (\Delta \theta)^2\}} \{\psi_{i+1,j+1} + \psi_{i-1,j-1} + \psi_{i-1,j+1} + \psi_{i+1,j-1} - 4\psi_{i,j}\}. \quad (31)$$

Similarly, the second-order approximation of diagonal discretized 9-point stencils concerning the radian axis:

$$\psi_{\theta\theta} = \frac{1}{3(\Delta\theta)^2} \{\psi_{i,j+1} - 2\psi_{i,j} + \psi_{i,j-1}\} + \frac{1}{3\{(\Delta r)^2 + (\Delta\theta)^2\}} \{\psi_{i+1,j+1} + \psi_{i-1,j-1} + \psi_{i-1,j+1} + \psi_{i+1,j-1} - 4\psi_{i,j}\}. \quad (32)$$

After substitution (27), (31) and (32) in (23), and doing some algebra, we have a 9-point isotropic stencil of Laplacian in polar mesh with a diagonal discretization technique.

$$\psi_{i,j} = w \left[\frac{1}{3(\Delta r)^2} \{\psi_{i+1,j} + \psi_{i-1,j}\} + \frac{1}{3\{(\Delta r)^2 + (\Delta\theta)^2\}} \{\psi_{i+1,j+1} + \psi_{i-1,j-1} + \psi_{i-1,j+1} + \psi_{i+1,j-1}\} + \frac{1}{6(r\Delta r)} \{\psi_{i+1,j} - \psi_{i-1,j}\} + \frac{1}{6r\sqrt{(\Delta r)^2 + (\Delta\theta)^2}} \{\psi_{i+1,j+1} - \psi_{i-1,j-1} + \psi_{i-1,j+1} - \psi_{i+1,j-1}\} + \frac{1}{3(r\Delta\theta)^2} \{\psi_{i,j+1} + \psi_{i,j-1}\} + \frac{1}{3r^2\{(\Delta r)^2 + (\Delta\theta)^2\}} \{\psi_{i+1,j+1} + \psi_{i-1,j-1} + \psi_{i-1,j+1} + \psi_{i+1,j-1}\} \right]. \quad (33)$$

The waiting factor w is: $w = \left[\frac{3(r\Delta r\Delta\theta)^2\{(\Delta r)^2 + (\Delta\theta)^2\}}{2\{(r\Delta\theta)^2 + (\Delta r)^2\}\{(\Delta r)^2 + (\Delta\theta)^2\} + 4\{r^2 + 1\}(\Delta r\Delta\theta)^2} \right]$ is the weighting factor of neighbouring and nearest neighbouring points. In this numerical scheme, i is taken as a discrete variable for the radial step and j is taken as a discrete variable representing an angular step in a polar grid system. However, $r_i \in \mathcal{R}$ and $\theta_j \in \mathcal{R}$.

3. Simulation, Results and Discussion

This study uses a cell dynamic simulation model using polar coordinates in a circular annular pore system. It investigates the diblock copolymers system to predict the emerging pattern of asymmetric Lamellae. The isotropic 9-point stencil of the Laplacian included in the CDS model is diagonally discretized, and the results are obtained in three steps. The first stage of the simulation examined the equilibrium distribution of the binary fluid in the macromolecule continuum of a diblock copolymer system to determine whether the distribution of materials in the system was based on diblock equilibrium. The second stage of the simulation is the prediction of the equilibrium phase of the lamellae formation process without attractive walls. The third stage of the simulation is the prediction of emerging Lamellae patterns with attractive walls.

3.1 Binary Fluid Simulations

In the CDS model, the simulation begins by assuming that the blocks of polymers in the system are evenly distributed over the total molecular weight of the material. For this purpose, the binary fluid mixture phase has been tested in the annular circular pore. The parameters used to test binary fluid simulations are given in Table 1:

Table 1: Binary fluid simulation of asymmetric AB-block copolymer melts using 9-point diagonally discretized Laplacian

u	v	f	τ	α	A	B	D
0.50	2.30	0.48	0.36	0.00	1.50	0.00	0.50

Macrophase separation from this simulation occurs when the material under the pore system mixes into separate A-rich and B-rich macrodomains, as shown in Figure 6. For binary fluid simulation, an annular circular pore system has been established by keeping the outer radius of the circular annular pore at 6 and the inner radius at 3. The simulation is run for one-million-time steps with a grid size $60 \times 360 \times 1$. The size of this pore system has been kept at 3. The results of the binary fluid test show that the domain is completely divided into two A-rich subdomains (Red) and B-rich subdomains (Blue).

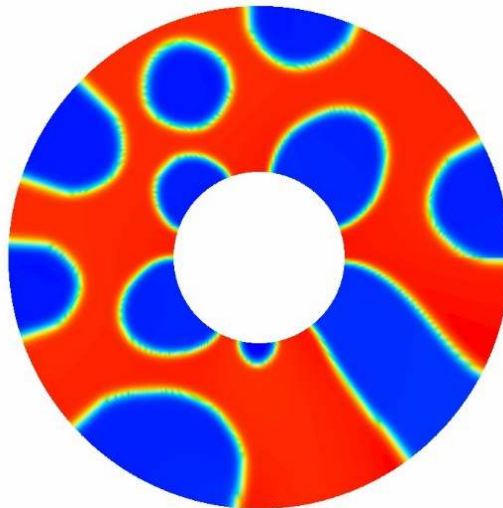


Figure 6: Binary fluid simulation of asymmetric diblock copolymer melt confined in annular circular pore.

3.2 Simulations of emerging Lamellae patterns with neutral walls

The two-dimensional investigation is carried out to study asymmetric lamellae forming systems of diblock copolymer melts in a circular angular pore of size $d = r_b - r_a$ having a fixed internal radius $r_a = 3, 5, 7$ and 9 and variable external radius r_b corresponding to the extended pore sizes

Table 2: CDS parameters for lamellae forming of symmetric AB-block copolymer melt without attractive walls

u	v	f	τ	α	A	B	D
0.50	2.30	0.50	0.36	0.00	1.50	0.02	0.50

The pore geometry consists of polar mesh for which periodic boundary conditions are applied in angular domains $[0, 2\pi]$ and reflective boundary conditions are applied in the radial domain. The simulation is run for one-million-time steps. The initial random statistical order parameter ψ belongs to $[-0.5, +0.5]$. The parameter is kept to zero for neutral wall simulations. The parameter values used in the CDS model for this investigation are given in Table 2.

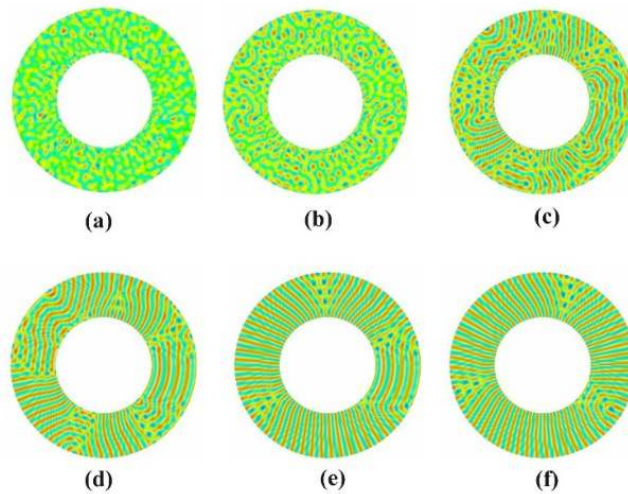


Figure 7: Simulation of asymmetric Lamellae patterning with neutral walls at various time steps

The evaluation of the cell dynamic simulations at different time steps is provided in Figure 7. The internal radius is fixed at $r_a = 3$ and the external radius is fixed at $r_b = 6$. The grid size is fixed at

$30 \times 360 \times 1$, to get pore size 6. The simulations are carried out up to 1000,000 steps. Figure 7 is a cluster of six patterns extracted over different time steps: $t = 10$ (a), $t = 100$ (b), $t = 1000$ (c), $t = 10000$ (d), $t = 100000$ (e) and $t = 1000000$ (f). The circular pore system has lamellae (thin layers) formed by curved geometry that predicts unique patterns. These patterns are affected by pore boundaries. The curvature causes lamellar distortion, and defects are also visible. Due to the minimum amount of free energy during interaction with the pore walls to form lamellae, equilibrium is reached, and the system converges and stabilizes, forming lamellar patterns.

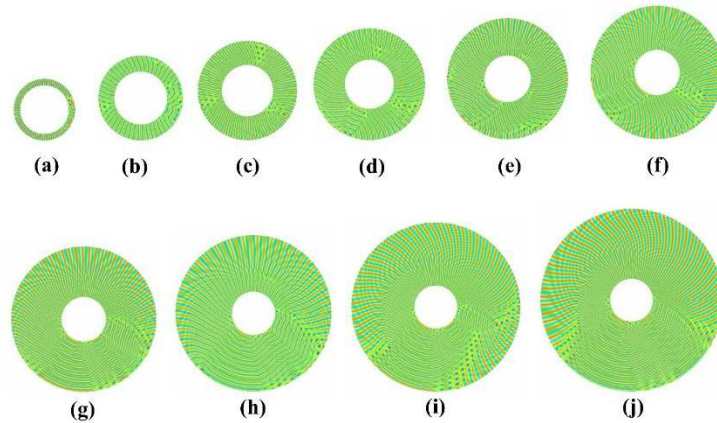


Figure 8: Simulation of asymmetric Lamellae patterning at $r_a = 3$ with neutral walls

Figure 8 presents the asymmetric lamellae forming system in an annular circular pore without attractive walls in which $r_a = 3$ and $r_b = \{4,5,6,7,8,9,10,11,12,13\}$ to get extended pore sizes $d = \{1,2,3,4,5,6,7,8,9,10\}$.

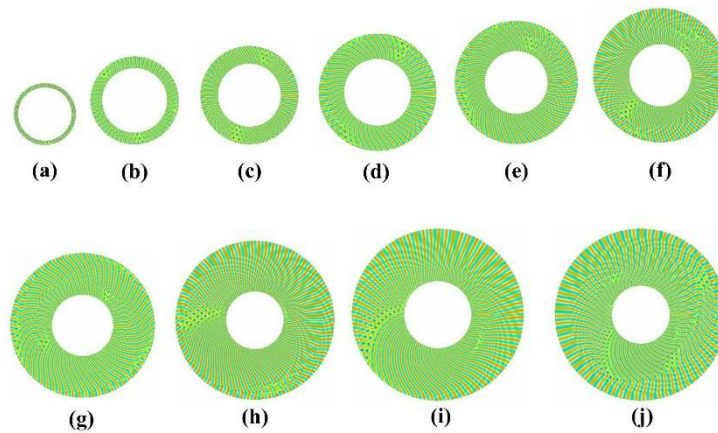


Figure 9: Simulation of asymmetric Lamellae patterning at $r_a = 5$ with neutral walls

Figure 9 shows the asymmetric lamellae forming system in an annular circular pore without attractive walls. The internal radius of the pore is fixed at $r_a = 5$. The external radius of the pore is varied according to $r_b = \{6,7,8,9,10,11,12,13,14,15\}$ to get extended various pore sizes $d = \{1,2,3,4,5,6,7,8,9,10\}$.

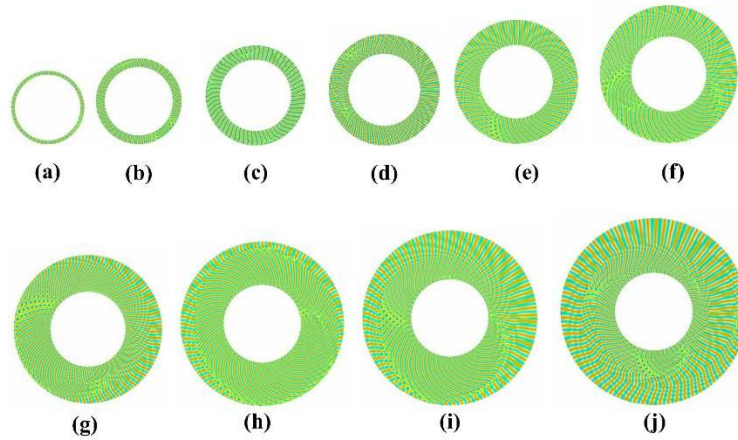


Figure 10: Simulation of asymmetric Lamellae patterning at $r_a = 7$ with neutral walls

Figure 10 presents the asymmetric lamellae forming system in an annular circular pore without attractive walls in which $r_a = 7$ and $r_b = \{8,9,10,11,12,13,14,15,16,17\}$ to get extended pore sizes $d = \{1,2,3,4,5,6,7,8,9,10\}$.

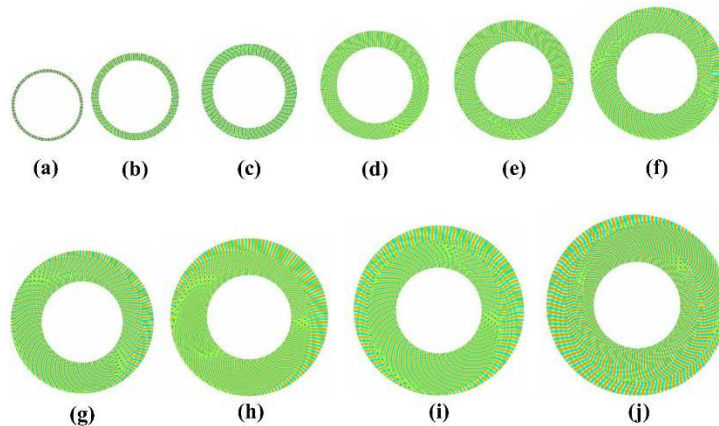


Figure 11: Simulation of asymmetric Lamellae patterning at $r_a = 9$ with neutral walls

Figure 9 shows the asymmetric lamellae forming system in an annular circular pore without attractive walls. The internal radius of the pore is fixed at $r_a = 5$. The external radius of the pore is varied according to $r_b = \{6,7,8,9,10,11,12,13,14,15\}$ to get extended various pore sizes $d = \{1,2,3,4,5,6,7,8,9,10\}$.

Investigating the effect of film thickness and curvature, the grain boundary morphology is visible, along with perforated holes and curved parallel lamellae to the pore. This shows a significant effect of curvature and confinement. The Lamella forming system has been researched in the diblock copolymer system by keeping the inner radius at 3, 5, 7, and 9 for pore sizes; the results revealed that due to the effect of curvature and gradually increasing the inner radius, the lamellae paradigms have been realized in farming systems. Perforated holes are found, pore-parallel wavy lamellae patterns are also seen, and at some places, vertical lamellae of Moore are also found; grain boundary morphology is found at almost every pore size, and some defects are also observed. In some cases, dislocation and disinclination morphologies are also observed.

3.3 Simulations of emerging Lamellae patterns with attractive walls

In this phase of simulation, the lamellae forming system is investigated under confinement by imposing interfacial attractive wall strength $\alpha = 0.2$. Table 3 gives the parameters of the CDS model employed for confined asymmetric diblock copolymer in circular annular pores.

Table 4: CDS parameters for lamellae forming of symmetric AB-DBC melt

u	v	f	τ	α	A	B	D
0.50	2.30	0.50	0.36	0.2	1.50	0.02	0.50

The polar mesh is based on radial and radian domains. The radian domains are subject to periodic boundary conditions, the radial domains are subject to reflective boundary conditions, and confinement in melt is subject to symmetric boundary conditions. The simulations are run for one million time steps to investigate the effect of one-dimensional confined diblock copolymer melts in annular circular pores. In Figure 12, the evaluation of the lamellae forming system in asymmetric diblock copolymers under one-dimensional confinement in the annular circular pore is present after different time steps. The internal radius is fixed at $r_a = 3$ and the outer radius is

fixed at $r_b = 6$ to get pore size $d = r_b - r_a = 3$. The interfacial wall's strength is fixed at $\alpha = 2$. Figure 12 presents a group of six patterns extracted over different time steps: $t = 10$ (a), $t = 100$ (b), $t = 1000$ (c), $t = 10000$ (d), $t = 100000$ (e) and $t = 1000000$ (f).

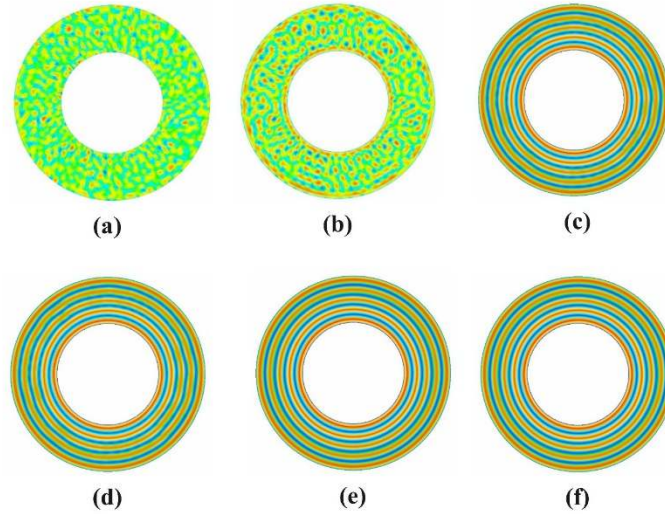


Figure 12: Simulation of confined asymmetric lamellae patterning at various time steps

A microphase separation occurs instead of macrophase separation, deriving the self-assembly to compete between the system's entropy and enthalpy. Minimization of free energy increases the degree of segregation, resulting in concentric circular lamellae.

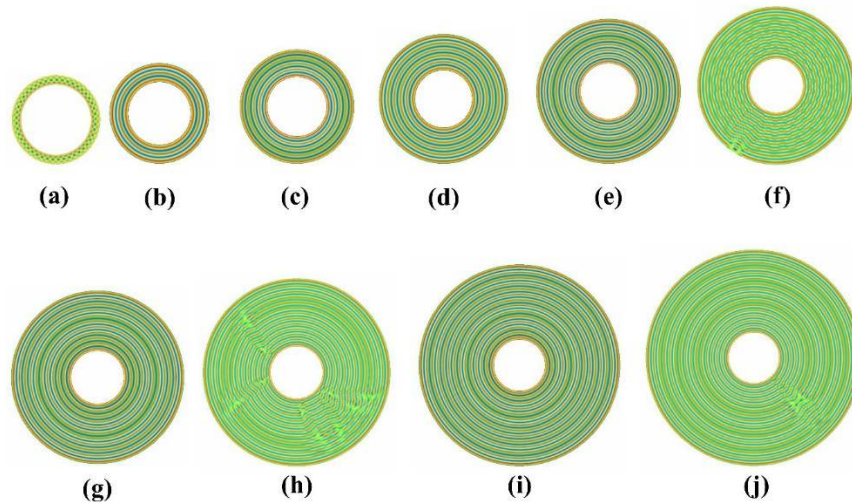


Figure 13: Simulation of asymmetric Lamellae patterning at $r_a = 3$ with attractive walls

Figure 13 presents the lamellae forming system confined in an annular circular pore with attractive walls for various pore sizes. The internal radius of the pore is fixed at $r_a = 3$.

The variable external radius of the pore is $r_b = 4,5,6,7,8,9,10,11,12,13$; to get extended pore sizes $d = 1,2,3,4,5,6,7,8,9,10$.

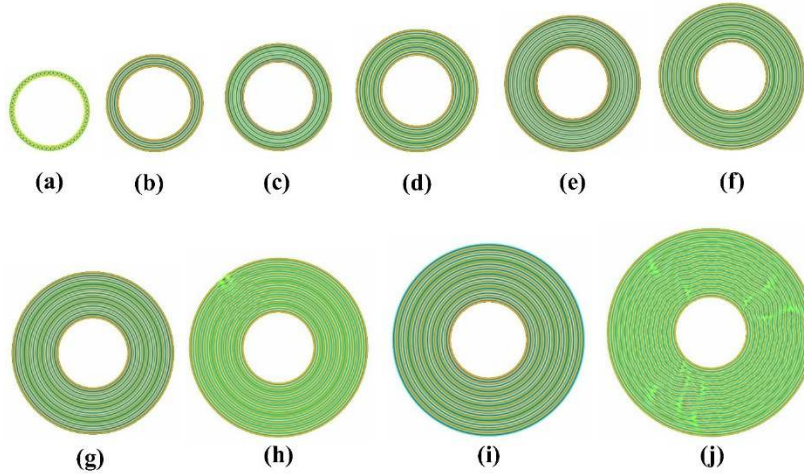


Figure 14: Simulation of asymmetric Lamellae patterning at $r_a = 5$ with attractive walls

Figure 13 presents the lamellae forming system confined in an annular circular pore with attractive walls for various pore sizes. The internal radius of the pore is fixed at $r_a = 5$. The variable external radius of the pore is $r_b = 6,7,8,9,10,11,12,13,14,15$; to get extended pore sizes

$d = 1,2,3,4,5,6,7,8,9,10$.

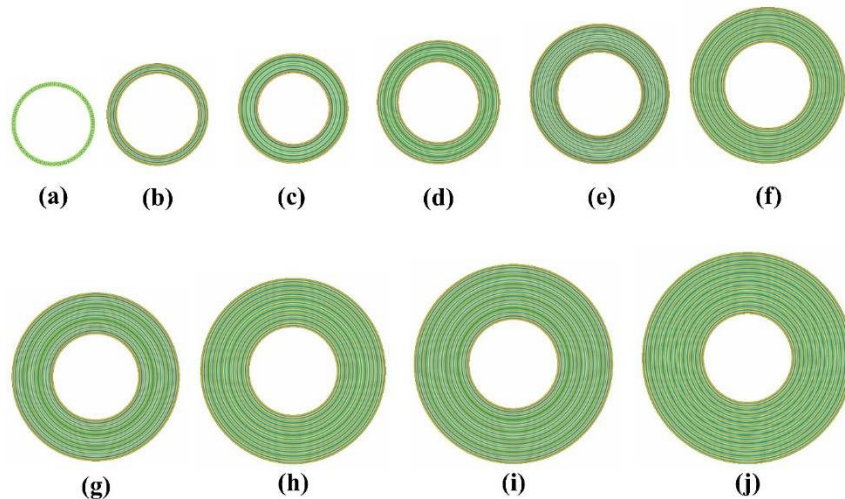


Figure 14: Simulation of asymmetric Lamellae patterning at $r_a = 7$ with attractive walls

Figure 14 presents the lamellae forming system confined in an annular circular pore for various pore sizes and attractive walls. The internal radius of the pore is fixed at $r_a = 7$. The variable external radius of the pore is $r_b = 8,9,10,11,12,13,14,15,16,17$; to get extended pore sizes $d = 1,2,3,4,5,6,7,8,9,10$.

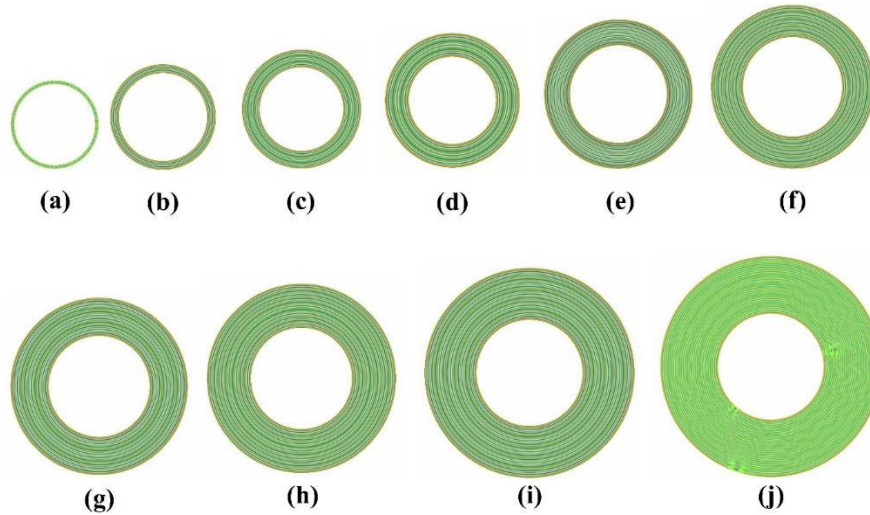
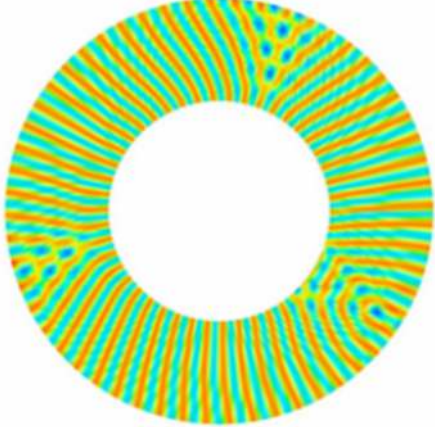
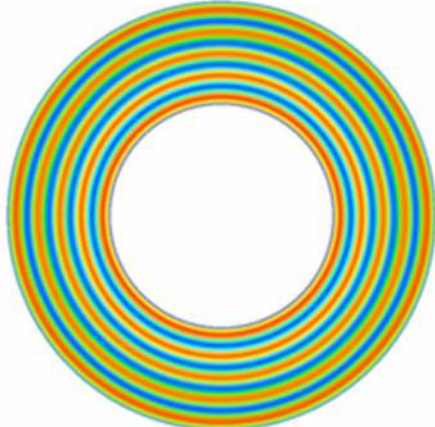


Figure 15: Simulation of asymmetric Lamellae patterning at $r_a = 9$ with attractive walls

Figure 15 presents the lamellae forming system confined in an annular circular pore for various pore sizes with attractive walls. The internal radius of the pore is fixed at $r_a = 9$. The variable external radius of the pore is $r_b = 10,11,12,13,14,15,16,17,18,19$; to get extended pore sizes $d = 1,2,3,4,5,6,7,8,9,10$.

Diblock copolymer melts have been subjected to simulation steps with the CDS model and investigated for the effects of confinement and curvature in the annular circular pore system of the lamella forming system. The effects of curvature and confinement and pore sizes at different values of inner radius have also been examined. According to the results, due to the affinity between a block and the whole surface of the system in diblock copolymers, there is competition in the entropy and enthalpy of the system due to the reduction of the free energy, which helps to transform the disordered state into the ordered state. Some anomalies and defects have also come to light. Concentric circular lamella formation due to curvature and confinement resulted in dot-board morphology lamellae whose number is proportional to the grid size. Concentric circles of lamellae are significant due to pore sizes and inner radius.

4. Comparison with other studies

Investigated Lamellae forming system	Significance and consistency with other Investigations	
	<p>[54] Study of the ordered assembly morphologies of diblock copolymers on the same substrate</p>	<p>[55] Plasma etch transfer of self-assembled polymer patterns</p>
	<p>[56] Concentric lamella structures of symmetric diblock copolymers confined in cylindrical nanopores</p>	<p>[57] Fabrication of Nanodevices Through Block Copolymer Self- Assembly</p>

5. Conclusion

This computational investigation studies the lamellae-forming system of asymmetric diblock copolymer melts confined in polar geometries through a cell dynamic simulation model with the help of IFORT and OPEN Dx. The simulation is conducted for one million time steps. The macromolecule of diblock copolymer melts is diagonally discretized by newly constructed efficient 9-point stencils in polar mesh. The study is conducted in three phases. In the first phase, the macrophase separation mechanism is studied for binary fluid simulations to observe how the continuum molecule is converted into two subdomains having A-rich and B-rich concentrations of

diblock copolymer melts. In the second phase, the lamellae-forming system is investigated for diblock copolymer melts in concentric circles without interfacial walls. The simulation results show perforated holes, grain boundary, dislocation, and disinclination morphologies. The lamellae-forming system is investigated in geometrical confinement with interfacial walls in the third investigation phase. The simulation results show dartboard morphologies consistent with other investigations.

Bibliography

- [1] Sahu, M. K., Yadav, R., & Tiwari, S. P. (2023). Recent advances in nanotechnology. *International Journal of Nanomaterials, Nanotechnology and Nanomedicine*, 9(1), 015-023.
- [2] Malik, S., Muhammad, K., & Waheed, Y. (2023). Nanotechnology: A revolution in modern industry. *Molecules*, 28(2), 661.
- [3] Kricka, L. J., & Fortina, P. (2002). Nanotechnology and applications: an all-language literature survey including books and patents. *Clinical chemistry*, 48(4), 662-665.
- [4] Bobokulova, M. (2024). THE ROLE OF NANOTECHNOLOGY IN MODERN PHYSICS. *Development and innovations in science*, 3(1), 145-153.
- [5] Dua, S., Ahmed, H., & Arfin, N. (2023). Soft nanomaterials and their applications. In *Nanomaterials: the building blocks of modern technology: synthesis, properties and applications* (pp. 27-68). Singapore: Springer Nature Singapore.
- [6] Barrat, J. L., Del Gado, E., Egelhaaf, S. U., Mao, X., Dijkstra, M., Pine, D. J., ... & Kwon, J. (2023). Soft matter roadmap. *Journal of Physics: Materials*, 7(1), 012501.
- [7] Van Saarloos, W., Vitelli, V., & Zeravcic, Z. (2024). *Soft Matter: Concepts, Phenomena, and Applications*. Princeton University Press.
- [8] Langevin, D. (2023). An Adventure into the World of Soft Matter. *Annual Review of Condensed Matter Physics*, 14, 21-33.
- [9] Bang, R. S., Roh, S., Williams, A. H., Stoyanov, S. D., & Veleev, O. D. (2023). Fluid Flow Templating of Polymeric Soft Matter with Diverse Morphologies. *Advanced Materials*, 35(16), 2211438.
- [10] Lazzari, M., & Torneiro, M. (2020). A global view on block copolymers. *Polymers*, 12(4), 8

- [11] Xie, J., & Shi, A. C. (2023). Theory of Complex Spherical Packing Phases in Diblock Copolymer/Homopolymer Blends. *Macromolecules*, 56(24), 10296-10312.
- [12] Patterson, A. L., Yu, B., Danielsen, S. P., Davidson, E. C., Fredrickson, G. H., & Segalman, R. A. (2020). Monomer sequence effects on interfacial width and mixing in self-assembled diblock copolymers. *Macromolecules*, 53(9), 3262-3272.
- [13] Koltzenburg, S., Maskos, M., & Nuyken, O. (2023). *Polymer Chemistry*. Springer Nature.
- [14] Armes, S. P., Perrier, S., & Zetterlund, P. B. (2021). Introduction to polymerisation-induced self-assembly. *Polymer Chemistry*, 12(1), 8-11.
- [15] Abetz, V. (2020). Self-Assembly of Block Copolymers. *Polymers*, 12(4), 794.
- [16] Gan, Z., Zhou, D., Ma, Z., Xu, M., Xu, Z., He, J., ... & Dong, X. H. (2022). Local chain feature mandated self-assembly of block copolymers. *Journal of the American Chemical Society*, 145(1), 487-497.
- [17] Kim, K. H., Huh, Y., Song, I., Ryu, D. Y., Son, J. G., & Bang, J. (2024). Recent advances in block copolymer self-assembly: From the lowest to the highest. *Journal of Polymer Science*, 62(4), 679-692.
- [18] Li, Z., & Lin, Z. (2022). Self-assembly of block copolymers for biological applications. *Polymer International*, 71(4), 366-370.
- [19] Iqbal, M. J., Soomro, I., Bibi, M., & Mallah, R. N. (2023). Morphological Investigation of Lamellae Patterns in Diblock Copolymers under Change of Thickness and Confinement in Polar Geometry. *VFAST Transactions on Mathematics*, 11(2), 174-197.
- [20] Hagita, K., & Murashima, T. (2024). Coarse-grained molecular dynamics model of AB diblock copolymers composed of blocks with different Lennard-Jones parameters forming lamellar structures. *Polymer*, 127132.
- [21] Woo, D., Yoon, H., & Kim, J. K. (2024). Unconventional microdomains of block copolymers. *Journal of Polymer Science*, 62(4), 639-661.
- [22] Xie, J., & Shi, A. C. (2023). Theory of Complex Spherical Packing Phases in Diblock Copolymer/Homopolymer Blends. *Macromolecules*, 56(24), 10296-10312.
- [23] Qu, T., Hu, X., Zhou, Z., Liu, Y., Wang, J., Hu, F., ... & Liu, H. (2023). Morphology Control of Perpendicularly Oriented Lamellar Films from Azobenzene-Containing Block

- Copolymers with Different Spacer Lengths. *The Journal of Physical Chemistry C*, 127(7), 3882-3889.
- [24] Lee, H., Kim, J., & Park, M. J. (2024). Exploration of complex nanostructures in block copolymers. *Physical Review Materials*, 8(2), 020302.
- [25] Li, W., Liu, M., Qiu, F., & Shi, A. C. (2013). Phase diagram of diblock copolymers confined in thin films. *The Journal of Physical Chemistry B*, 117(17), 5280-5288.
- [26] Schneider, L., & Müller, M. (2019). Rheology of symmetric diblock copolymers. *Computational Materials Science*, 169, 109107.
- [27] Yan, N., Song, Y., & Zhu, Y. (2023). Confined self-assembly of block copolymers in emulsion droplets: Preparation, shape and internal structure, and applications. *Journal of Polymer Science*, 61(24), 3211-3227.
- [28] Pester, C. W., Liedel, C., Ruppel, M., & Böker, A. (2017). Block copolymers in electric fields. *Progress in Polymer Science*, 64, 182-214.
- [29] Merkalov, A. S., Derikov, Y. I., Artemov, V. V., Ezhov, A. A., & Kudryavtsev, Y. V. (2021). Vertical cylinder-to-lamella transition in thin block copolymer films induced by in-plane electric field. *Polymers*, 13(22), 3959.
- [30] Majewski, P. W., Gopinadhan, M., & Osuji, C. O. (2012). Magnetic field alignment of block copolymers and polymer nanocomposites: Scalable microstructure control in functional soft materials. *Journal of Polymer Science Part B: Polymer Physics*, 50(1), 2-8.
- [31] Singh, Maninderjeet, et al. "Directed Self-assembly of Block Copolymers with Dynamic Thermal Gradients." *Soft Matter and Biomaterials on the Nanoscale: The WSPC Reference on Functional Nanomaterials—Part I Volume 2: Polymers on the Nanoscale: Nano-structured Polymers and Their Applications*. 2020. 373-409.
- [32] Yu, B., Sun, P., Chen, T., Jin, Q., Ding, D., Li, B., & Shi, A. C. (2006). Confinement-induced novel morphologies of block copolymers. *Physical review letters*, 96(13), 138306.
- [33] Inayatullah Soomro, I. A., Shah, S. B., Majid, A., Muhammad, R., Hameed, A., Abas, G., ... & Ahmed, W. (2019). Mathematical Modelling of Cylindrical Forming Di-block Copolymers confined in circular annular pores. *IJCSNS*, 19(2), 16.

- [34] Iqbal, M. J., Soomro, I., Mahar, M. H., & Gulzar, U. (2024). Exploring Long-Range Order in Diblock Copolymers through Cell Dynamic Simulations. *VFAST Transactions on Software Engineering*, 12(2), 31-45.
- [35] Iqbal, M. J., Soomro, I., Bibi, M., & Mallah, R. N. (2023). Morphological Investigation of Lamellae Patterns in Diblock Copolymers under Change of Thickness and Confinement in Polar Geometry. *VFAST Transactions on Mathematics*, 11(2), 174-197.
- [36] Iqbal, M. J., Soomro, I., & Gulzar, U. (2024). Patterns of nanoporous spherical packing emerging under influence of curvature and confinement. *VFAST Transactions on Mathematics*, 12(1), 121-136.
- [37] Iqbal, M. J., Soomro, I., & Mahar, M. H. (2024). Re-patterning of cylindrical packing of diblock copolymers under confinement and curvature effects by using approximations of PDE's involved in the CDS model on polar mesh system. *Journal of Physics Communications*, 8(8), 085001.
- [35] Hamley, I. W. (2000). Cell dynamics simulations of block copolymers. *Macromolecular theory and simulations*, 9(7), 363-380.
- [36] Krausch, G., & Magerle, R. (2002). Nanostructured thin films via self-assembly of block copolymers. *Advanced Materials*, 14(21), 1579-1583.
- [37] Xie, P., Xu, M., Dong, Q., Song, Q., & Liu, M. (2024). Stabilizing undulated lamellae by diblock copolymers confined in alternately adsorbed thin films. *Giant*, 17, 100219.
- [38] He, X., Liang, H., Song, M., & Pan, C. (2002). Possibility of Design of Nanodevices by Confined Macromolecular Self-Assembly. *Macromolecular theory and simulations*, 11(4), 379-382.
- [39] Sevink, G. J. A., Zvelindovsky, A. V., Fraaije, J. G. E. M., & Huinink, H. P. (2001). Morphology of symmetric block copolymer in a cylindrical pore. *The Journal of Chemical Physics*, 115(17), 8226-8230.
- [40] Feng, J., Liu, H., & Hu, Y. (2006). Mesophase separation of diblock copolymer confined in a cylindrical tube studied by dissipative particle dynamics. *Macromolecular theory and simulations*, 15(9), 674-685.

- [41] Wang, Q. (2007). Monte Carlo simulations of nano-confined block copolymers. In *Nanostructured Soft Matter: Experiment, Theory, Simulation and Perspectives* (pp. 495-527). Dordrecht: Springer Netherlands.
- [42] Schmid, F., & Li, B. (2020). Dynamic self-consistent field approach for studying kinetic processes in multiblock copolymer melts. *Polymers*, 12(10), 2205.
- [43] Xiang, W., Zhu, Z., Wang, K., & Zhou, L. (2019). Mesoscopic simulation study on the structural transition of comb-shaped block copolymer lamellae on chemically patterned substrates: from vertical to lateral. *Physical Chemistry Chemical Physics*, 21(2), 641-649.
- [44] Kim, S., Lee, J., Jeon, S. M., Lee, H. H., Char, K., & Sohn, B. H. (2008). Orientation of lamellar nanostructures in the patterned thin films of a diblock copolymer. *Macromolecules*, 41(10), 3401-3404.
- [45] Aissou, K., Kwon, W., Mumtaz, M., Antoine, S., Maret, M., Portale, G., ... & Hadziioannou, G. (2016). Archimedean Tilings and Hierarchical Lamellar Morphology Formed by Semicrystalline Miktoarm Star Terpolymer Thin Films. *ACS nano*, 10(4), 4055-4061.
- [46] Xia, Y., & Li, W. (2019). Defect-free hexagonal patterns formed by AB diblock copolymers under triangular confinement. *Polymer*, 166, 21-26.
- [47] Xie, P., Xu, M., Dong, Q., Song, Q., & Liu, M. (2024). Stabilizing undulated lamellae by diblock copolymers confined in alternately adsorbed thin films. *Giant*, 17, 100219.
- [48] Dimitriyev, M. S., Reddy, A., & Grason, G. M. (2023). Medial packing, frustration, and competing network phases in strongly segregated block copolymers. *Macromolecules*, 56(17), 7184-7202.
- [49] Laradji, M., Shi, A. C., Noolandi, J., & Desai, R. C. (1997). Stability of ordered phases in diblock copolymer melts. *Macromolecules*, 30(11), 3242-3255.
- [50] Ohta, T., & Kawasaki, K. (1986). Equilibrium morphology of block copolymer melts. *Macromolecules*, 19(10), 2621-2632.
- [51] Ohta T and Kawasaki K 1986 Equilibrium morphology of block copolymer melts *Macromolecules* 19 2621-32

- [52] Zvelindovsky, A. V. (Ed.). (2007). Nanostructured soft matter: experiment, theory, simulation and perspectives. Springer Science & Business Media.
- [53] Hamley, I. W. (2000). Cell dynamics simulations of block copolymers. *Macromolecular theory and simulations*, 9(7), 363-380.
- [54] Zhang, B., Meng, L., & Li, Z. (2022). Study of the ordered assembly morphologies of diblock copolymers on the same substrate. *RSC advances*, 12(44), 28376-28387.
- [55] Johnston, D. E., Lu, M., & Black, C. T. (2012). Plasma etch transfer of self-assembled polymer patterns. *Journal of Micro/Nanolithography, MEMS, and MOEMS*, 11(3), 031306-031306.
- [56] Li, S., Wang, X., Zhang, L., Liang, H., & Chen, P. (2009). Concentric lamella structures of symmetric diblock copolymers confined in cylindrical nanopores. *Polymer*, 50(21), 5149-5157.
- [57] Hu, X. H., & Xiong, S. (2022). Fabrication of nanodevices through block copolymer self-assembly. *Frontiers in Nanotechnology*, 4, 762996.